Nationaal Lucht- en Ruimtevaartlaboratorium
National Aerospace Laboratory NLR

NLR-TP-2000-378

Demonstration of viscous flow computations on hybrid (prismatic/tetrahedral) grids

J.W. van der Burg, K.M.J. de Cock and S.P. van der Pijl

Nationaal Lucht- en Ruimtevaartlaboratorium
National Aerospace Laboratory NLR

NLR-TP-2000-378

Demonstration of viscous flow computations on hybrid (prismatic/tetrahedral) grids

J.W. van der Burg, K.M.J. de Cock and S.P. van der Pijl

This work has been carried out in NLR's basic research programme, Workplan Number A.1.B.2.

This report is based on a presentation held at the 7th International Conference on Numerical Grid Generation in Computational Field Simulations, Whistler, Canada, September 2000.

The contents of this report may be cited on condition that full credit is given to NLR and the authors.

Division:	Fluid Dynamics
Issued:	July 2000
Classification of title:	Unclassified

Abstract

Hybrid grid technology has become an important tool for aerodynamic analysis and design because of the high level of automation. At NLR a hybrid grid CFD system[1] for computing viscous flows around complex aircraft configurations is deployed in aerodynamic project work. In the paper an overview is presented of the current capabilities of the CFD system among which are three-dimensional hybrid grid generation, viscous flow modelling and grid adaptation. The high automation level of grid generation for geometrically complex aircraft has increased CAD-modelling work.

[1] The FASTFLO CFD system has been developed in the frame of the DLR-NLR co-operation "CFD for Complete Aircraft" and the Brite-Euram fourth framework project FASTFLO II (Contract No. BRPR-CT97-0576) with partners DLR, FFA, SAAB, DASA, IBK and TU-Delft.

Contents

(15 pages in total)

1 Introduction

Viscous flow calculations for complex aircraft configurations have become feasible due to the application of hybrid grid technology. A short CFD problem turnaround time for complex aircraft configurations has been realised due to introduction of unstructured grid generation techniques which allow a higher level of automation in comparison with the more commonly used, conventional multi-block grid generation techniques.

2 CFD geometry modelling

In an aerodynamic project the CAD-geometry of an aircraft configuration is usually received from an aircraft manufacturer. To be able to carry out a viscous flow analysis for a geometrically complex aircraft configuration it is of importance to analyse and understand the aerodynamic geometry. In the geometry of an aircraft many wanted and unwanted details can be present, such as for instance: finite trailing edges, small holes and gaps, small curves, small surfaces patches, sharp angled surface patches. Before carrying out a viscous flow analysis these geometrical issues have to be handled.
Based on such a geometric analysis aerodynamically relevant and non-relevant parts of the geometry are identified. It can be decided to locally modify the geometry and to remove unwanted small-scale geometric features. A critical issue that then still remains is the accurate modelling of the geometry. In order to understand this better the concept of CFD geometry is introduced here.
The starting point of the FASTFLO CFD system (see Figure 1) is a geometry definition that from now on is referred to as the **CFD geometry**. The CFD geometry is defined as the CAD-geometry that consists of a collection of surfaces and trim curves describing all relevant aerodynamic parts and that is topologically and also preferably physically airtight.
Various ‘sending’ CAD systems are used nowadays by aircraft manufactures to define a general CAD/CAM geometry of an aircraft configuration and various ‘receiving’ systems are used to prepare a CFD geometry. At NLR ICEM CFD and a CAD-interface algorithm are utilised to produce an airtight geometry. In CAD systems, cloud of points, drawings, or existing geometry definitions can be used to generate, reshape, add, delete, intersect and trim surface patches, such that an airtight geometry results.
The geometry definition should contain information concerning the relation between the curves and surfaces in the geometry often referred to as topological information. In general three methods exist to produce this topological information:

1) By a 'sending' CAD system, for instance by means of a solid model that contains the relevant topology information.
2) Interactively by hand using a CAD system (trimming surfaces).
3) Automatically, by algorithmically adding topology information to the CAD geometry.

For the hybrid grid CFD system a combination of methods 2 and 3 has been pursued. Modern solid modelling CAD systems (currently under development) are able to deliver topological information (and airtight surfaces) and therefore are potentially interesting alternatives (method 1).
Human factors can also play a role in preparing a CFD geometry. The degree of familiarisation with the geometry requirements of the 'receiving' system (e.g. the CAD system or the CFD system) and the CAD skills of the CAD specialist are a critical success factor in preparing the CFD geometry. Therefore, much emphasis has been placed on the relaxation of the geometry input requirements of the CFD system.

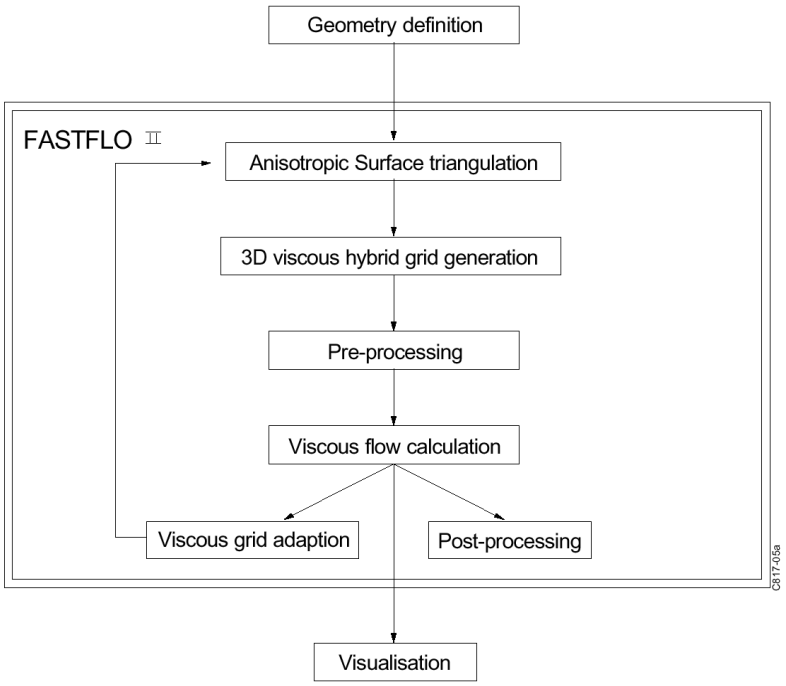

Fig. 1 Overview of the algorithmic components in the hybrid grid FASTFLO CFD system.

Care should be taken when exchanging a geometry definition between a 'sending' and 'receiving' system. Due to geometry exchange the geometry may be modified for several reasons [1]. These geometric changes have to be recognised and repaired by hand.

The hybrid grid CFD system supports a large range of geometries as input. The geometry can be defined either by the CAD data format IGES 5.1 or by the multi-block based format (structured surface patches).
The geometry is allowed to consist of a large number of curves and surface patches. Typically, in a complex aerodynamic configuration the number of surfaces is in the range of 200-1000. In figure 2 an example is shown of complex CFD-entities that are triangulated. The colours in this figure signify the individual surfaces. The number of curves is approximately in the range of 4-6 times the number of surfaces. Among the geometric options that are supported are singly and doubly curved NURBS surfaces that can either be trimmed or untrimmed.
Especially, the option that allows untrimmed surfaces in a geometry has alleviated the work of the CAD-specialist so that geometrically more complex configurations can be considered in the same time frame. Surfaces in the geometry definition that are intersecting, for instance a wing-body junction or a wing-pylon junction, should be trimmed (IGES 5.1 entity 144).
Small-scale geometric features are allowed in the geometry. Local tolerances have been introduced to support these features. Local tolerances are used to verify distances between points, curves and surfaces.

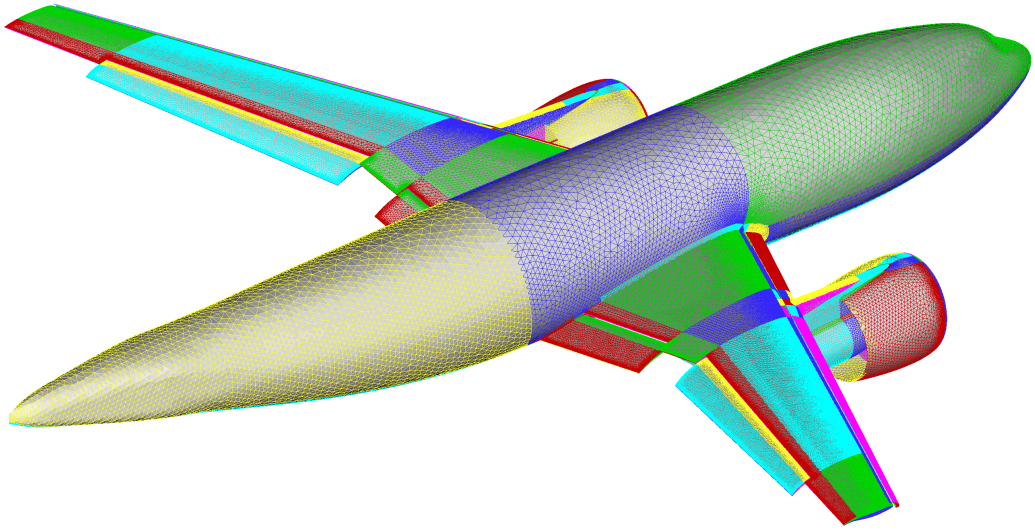

Fig. 2 Surface triangulation of the CFD geometry for the ALVAST high-lift configuration; The CFD geometry consists of 480 surfaces.

The CAD interface algorithm checks and verifies the geometric requirements with respect to the geometry defined in the IGES 5.1 format and extracts the geometry topology. In order to end up

with a topological airtight geometry for each pair of neighbouring surfaces an unique curve or chain of curves needs to be detected. For this purpose a trim curve splitting algorithm and an algorithm which verifies the distance between chains of curves is available. On termination of the algorithm a few curves may still be non-connected (due to a large specified tolerance). An option is offered to connect non-connected curves interactively.A tight and robust coupling to the IGES 5.1 CAD data format has ensured a large reduction in turnaround time compared to the multi-block approach.

3 Hybrid prismatic-tetrahedral grid generation

In order to be able to compute viscous flows a hybrid grid is generated in the three-dimensional flow domain. On the aerodynamic surfaces as defined by the CFD geometry a prismatic grid is produced in order to accurately capture the boundary layer. In the remaining part of the flow domain where viscous effects are less dominant a tetrahedral grid is created. The hybrid (prismatic/tetrahedral) grid generation algorithms are suited to handle the following types of aerodynamic configurations: a full model, a half model, a quasi two-dimensional-geometry model, multiple bodies and flat-plate like models. Flow domains representing an internal flow problem can also be handled.

For viscous flow calculations the chosen grid resolution is of major importance. In order to be able to accurately study the aerodynamic features for a specific aircraft configuration the parameters that define the grid should be carefully chosen. This can be a formidable task since a number of grid requirements have to be satisfied.

The first step in the formation of a ‘viscous’ hybrid grid is the surface triangulation of the CFD geometry. The surfaces of the CFD geometry are approximated by triangles which size is controlled by user-defined sources and/or surface curvature. Important here is that the aerodynamically relevant parts of the CFD geometry are accurately represented, which implies that firstly the CFD geometry itself is represented with sufficient accuracy and secondly that sufficient nodes/triangles are used to approximate the aerodynamic effects to be studied. On parts of the aerodynamic geometry where gradients are large such as on wing leading edges a centrally symmetric surface grid [2] is introduced (see Figure 3).

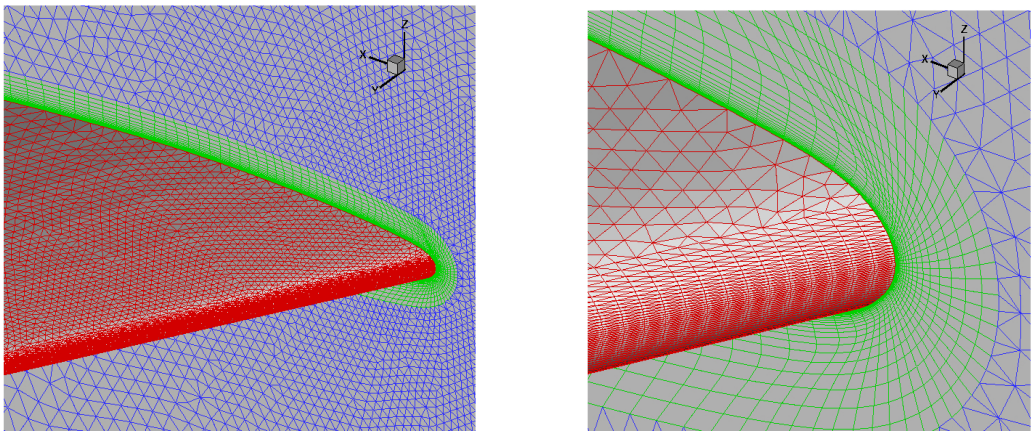

Fig. 3 Centrally symmetric surface grid at the leading edge for the ONERA M6 wing; Close-up at the wing leading edge.

To capture the near-wall viscous effects an initial prismatic grid based on the advancing layers approach [3,4,5] with a uniform height is generated on the aerodynamic surfaces of the aircraft configuration. The node distribution in the hybrid grid (and thus in the prismatic grid) can be improved later using grid adaptation based on local grid refinement and node movement. After prismatic grid generation the non-triangulated planes (symmetry planes and/or far field planes) of the flow domain are triangulated.

The next step tetrahedral grid generation consists of three parts. After the generation of an initial tetrahedral grid, nodes are automatically inserted into the tetrahedral grid based on a user-defined distribution function that controls the distance between the nodes in the grid. New nodes are connected to the grid by means of a positive-volume approach that guarantees that the volumes of the elements remain positive, see also [6]. A total memory of approximately 80 words per node is needed for the node insertion algorithm that is the maximum for all grid generation algorithms. In order to ensure a smooth transition of elements between the prismatic grid and the tetrahedral grid extra layers of grid nodes, distributed according the wall-normal stretching of the prismatic grid, can be inserted into the tetrahedral grid. Since the stability of the di-hedral angles of the tetrahedral elements in the grid cannot be maintained the grid should be optimised, see for instance [7]. The tetrahedral grid is optimised by adopting grid connectivity transformations and a redistribution algorithm [8].

Finally, by merging the prismatic grid and the tetrahedral grid a hybrid grid is formed. To each surface in the geometry a boundary identification is associated which will be used to select the boundary condition for this surface.

Short turnaround times for grid generation are guaranteed due to the incorporation of parallel processing in the grid generation algorithms for shared and distributed memory computers based on the MPI-library (see for instance [9]). For the surface triangulation algorithm (multi-block based) a load-balancing algorithm based on surface area size has been adopted to

decompose the workload for parallel execution. The automatic node insertion algorithm has been made suited for parallel processing as well. The decomposition of an initial grid is accomplished by inserting nodes located on planes of constant *x*. In between the planes of constant *x* a tetrahedral subgrid is generated. The final tetrahedral grid is obtained by merging the individual tetrahedral subgrids. As a result the time to generate a tetrahedral grid is significantly reduced.

4 Viscous flow calculation and grid adaption

Three-dimensional steady viscous flow in the CFD system is modelled based on the Reynolds-averaged Navier-Stokes equations. To account for turbulence the one-equation Spallart-Allmaras and the two-equation k-omega turbulence model are implemented. Transition from laminar to turbulent flow is enforced by means of boundary conditions. Engine inflow and outflow boundaries can be specified.
Since viscous flow computations on hybrid (prismatic/tetrahedral) grids for complex aircraft configurations are expensive in terms of computing time a supercomputer is needed to compute the steady viscous flow solution. At NLR the viscous flow computations are carried out on the NEC SX-5/8B supercomputer. This vector-computer possesses eight vector processors and has a shared main memory of 64 Gbyte. The peak speed is 8 Gflops per processor. Due to the edge-based data-structure adopted in the flow solver a good vector and parallel performance is realised on the NEC SX-5/8B.
In order to increase the grid resolution of the hybrid grid in regions of the flow domain where gradients are large a grid adaptation algorithm is employed. The grid adaptation algorithm is based on local grid refinement and node movement and utilises an equi-distribution grid adaptation algorithm that ensures that desirable flow features are not overlooked. In order to accurately represent the CFD geometry after grid adaptation new boundary nodes are projected onto the underlying IGES 5.1 surface of the CFD geometry.

5 Post-processing and visualisation

For the analysis of a viscous flow solution a post-processing algorithm for large-scale data is available. The post-processing algorithm allows an efficient computation of aerodynamic quantities and coefficients for the aerodynamic configuration under consideration. An advantage here is that the post-processing algorithm is installed on the NEC SX5/8B super computer ensuring short computation times. The post-processing algorithm has interfaces to visualisation software such as TecPlot and EnSight.

6 Applications

For three aircraft configurations the capabilities of the CFD system are illustrated. For an ONERA M6 wing, an AS28G wing-body configuration and a X31 test aircraft a fully turbulent viscous flow calculation has been performed with the Spallart-Allmaras turbulence model. In the viscous flow computations a convergence of three-orders of magnitude in residual has been realised.

For the ONERA M6 configuration a centrally symmetric surface grid at the leading edge of the wing is introduced (see Figure 3). The prismatic grid is specified such that the first layer corresponds to approximately $y^+ = 1$ (see Figures 3 and 7) and the height of the last prismatic layer matches the tetrahedral grid. From Figure 7 it can be observed that the computed viscous flow solution (on a hybrid grid having 1.7 million nodes and 40 prismatic grid layers) is in close agreement with a structured grid viscous flow solution.

For the AS28G wing-body configuration a centrally symmetric surface grid has been introduced at the leading edge of the wing (see Figure 4). The y^+-value for the first layer of the prismatic grid is chosen as 2. In Figure 8 it can be seen that the viscous flow solution (on a hybrid grid having 3 million nodes and 40 prismatic grid layers) is in agreement with experimental values (for sections $\eta = 0.229$ and $\eta = 0.477$).

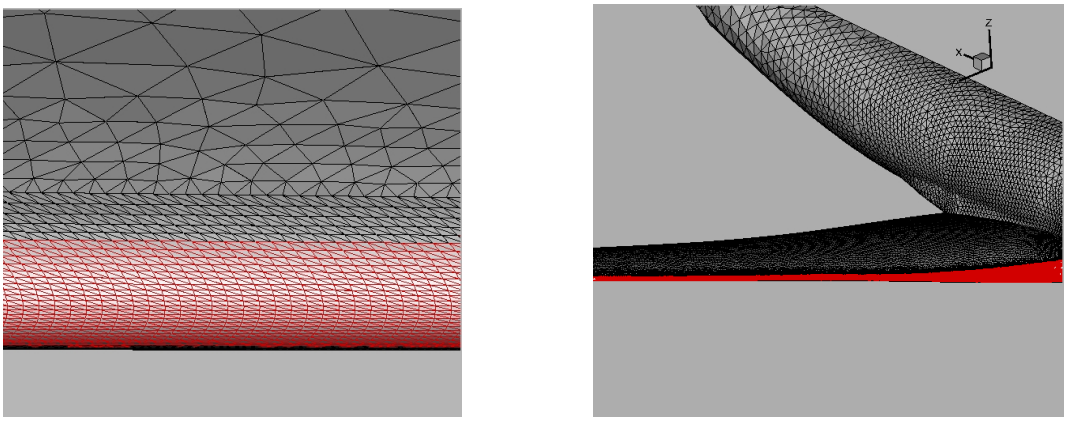

Fig. 4 Specification of a laminar flow region on the leading edge of the wing of the AS28G wing-body configuration

For the X31 test aircraft a viscous flow computation on a hybrid grid (having 4 million nodes and 20 prismatic grid layers) at high angle of attack is performed. In Figure 5 a close-up of the hybrid grid at the engine inlet area is shown. A valid prismatic grid is obtained in the inlet diverter area. In Figure 6 vortical structures can be observed on the canard and the wing. The CFD-problem-turnaround time starting from the CFD geometry for this configuration is within one week.

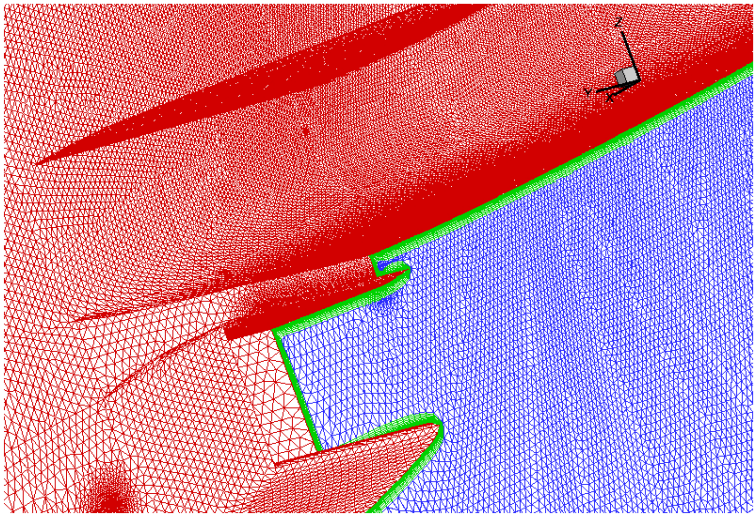

Fig. 5 Close-up of the surface grid at the inlet of the X31 test aircraft. The geometry definition of the X31 test aircraft has been received from DASA-M for use in the FASTFLO II-project.

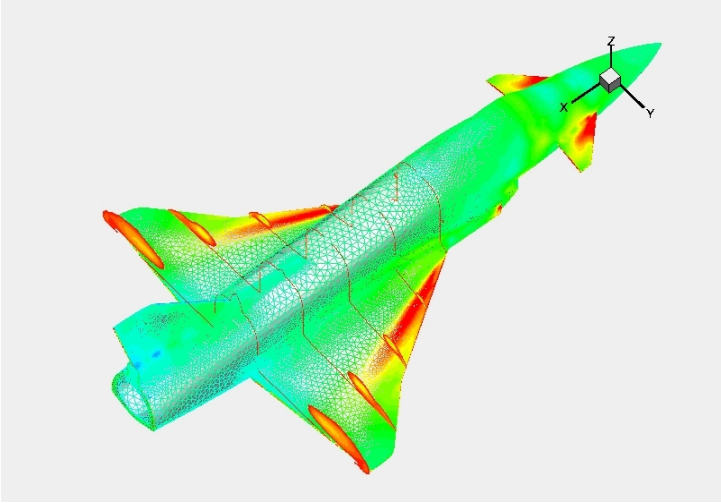

Fig. 6 Computed pressure distribution and visualisation of wing vortices (total pressure) on the X31-test aircraft for M=0.4 and α=20°, Re=4.0 $\times 10^7$. The geometry definition of the X31 test aircraft has been received from DASA-M for use in the FASTFLO II-project.

7 Conclusions

Due to the introduction of highly automated hybrid grid generation algorithms and viscous flow solver algorithms the major workload for carrying out a viscous flow calculation has been shifted from grid generation towards CFD geometry modelling and aerodynamic post-processing. CFD geometry modelling and CAD repair have become more important and more visible due to a higher level of automation in grid generation enabling CFD applications to more complex geometries.
Viscous flow capabilities are demonstrated for three configurations. For geometrically complex aircraft configurations the problem turnaround time remains within the order of one week. It has been shown that hybrid grid CFD can produce viscous flow solutions which agree well with computational (multi-block structured) and experimental results.

8 References

[1] Wulf, A., Steberl, R., Akdag, V; *"Efficient integration of CFD into product design"*, presented at the Industrial Computational Fluid Dynamics Conference, VKI, May 1999.

[2] Burg, J.W. van der, Maseland, J.E.J., Oskam, B.; *"Development of a fully automated CFD system for three-dimensional flow simulations based on hybrid prismatic/tetrahedral grids"*, NLR TP 96036 L, also in proceedings of the 5th International Conference On Numerical Grid Generation in Computational Field Simulations, Starkville, Mississippi, USA, April, 1996.

[3] Pirzadeh, S. *"Three-dimensional unstructured viscous grids by the advancing layers method"*, AIAA Journal, Vol. 34, No. 1, 1996.

[4] Kallinderis, Y., Khawaja, A., McMorris H., *"Hybrid prismatic/tetrahedral grid generation for viscous flows around complex geometries"*, AIAA Journal, Vol. 34, No. 2, 1996.

[5] Tysell, L., *"Hybrid grid generation for complex 3D geometries"*, in proceedings of the 7th International Conference on Grid Generation in Computational Field Simulation, Whistler, British Columbia, Canada, September, 2000.

[6] George, P.L., Hermeline, F. *"Delaunay's mesh of a convex polyhedron in dimension d. Application to arbitrary polyhedra"*, in proceedings of the 5th International Conference On Numerical Grid Generation in Computational Field Simulations, Starkville, Mississippi, USA, April, 1996.

[7] Baker, T.J., Vassberg, J.C., *"Tetrahedral Mesh Generation and Optimization"*, in proceedings of the 6th International Conference on Grid Generation in Computational Field Simulation, Greenwich, United Kingdom, July, 1998.

[8] Burg, J.W. van der, *"Tetrahedral grid optimisation: towards a structured tetrahedral grid"*, NLR TP-2000-343, also in proceedings of the 7th International Conference on Grid

Generation in Computational Field Simulation, Whistler, British Columbia, Canada, September, 2000.

[9] M.J. Marchant, N.P. Weatherill, E.A. Turner-Smith, Y. Zheng, M. Sotirakis., *"A Parallel Simulation User Environment for Computational Engineering"*, in proceedings of the 5th International Conference On Numerical Grid Generation in Computational Field Simulations, Starkville, Mississippi, USA, April, 1996.

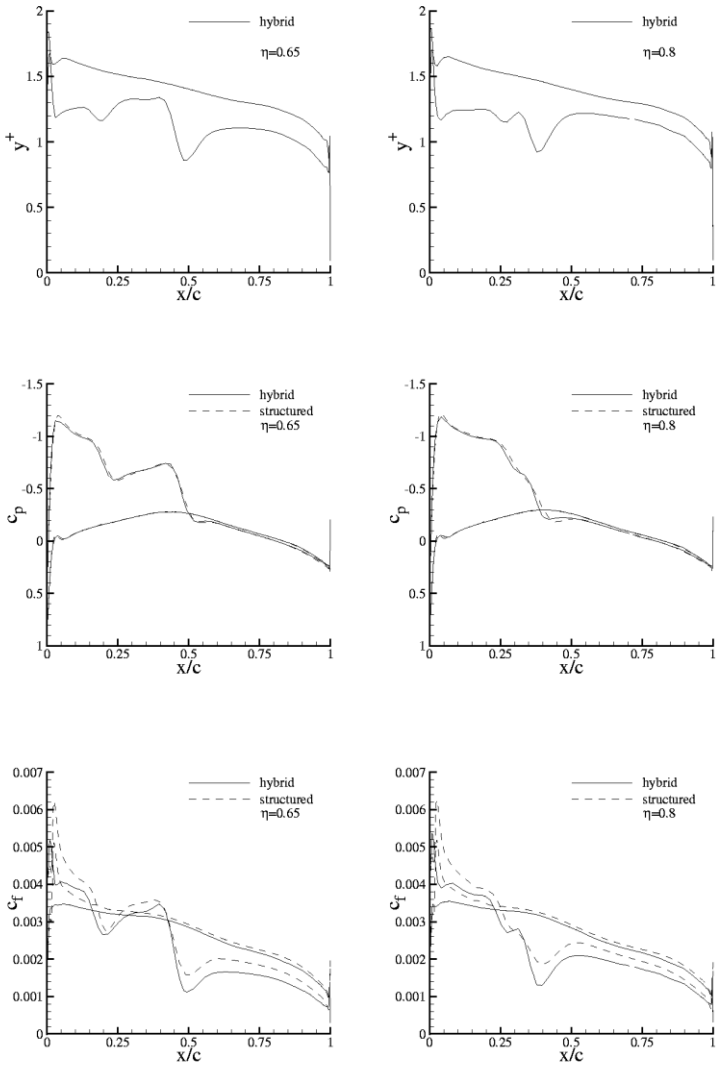

Fig. 7 Comparison of hybrid and structured grid solutions for the ONERA M6 wing; Distribution of y^+, pressure and skin friction coefficient for the sections 0.65 and 0.8.

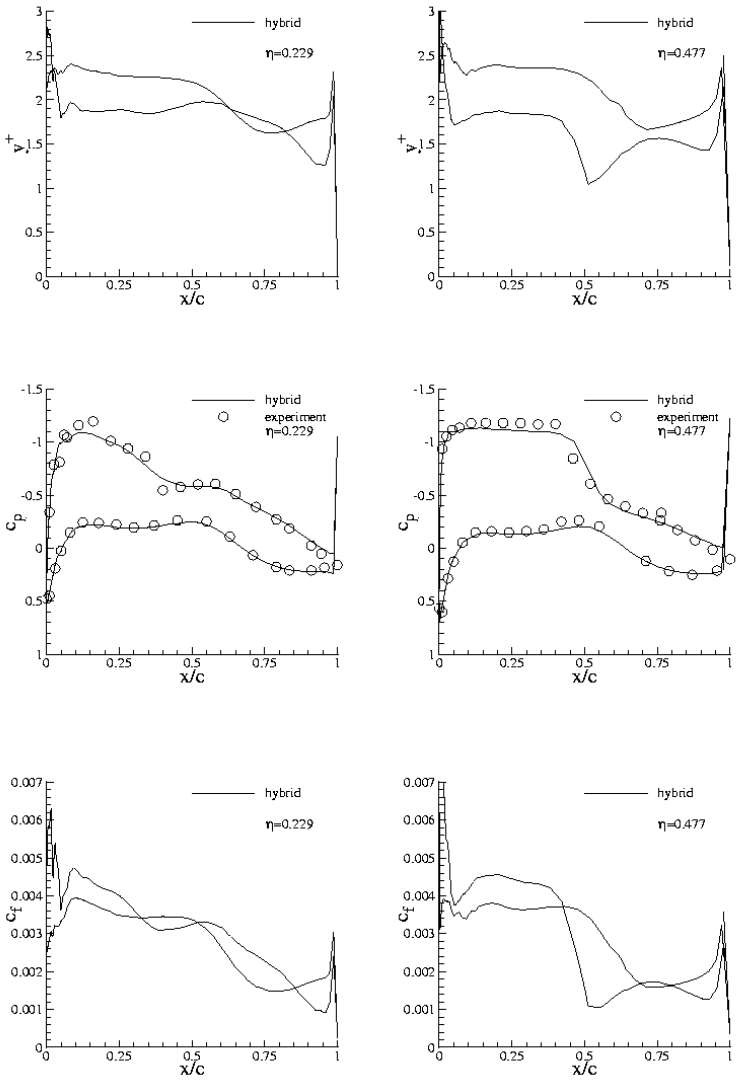

Fig. 8 Comparison of the viscous flow solution and the experiment for the AS28G wing-body; Distribution of y^+, pressure and skin friction coefficient for the sections 0.229 and 0.477.